Nonreducing terminal chimeric isomaltomegalosaccharide and its integration with azoreductase for the remediation of soil-contaminated lipophilic azo dyes

Weeranuch Lang[1,*], Sarote Sirisansaneeyakul[2], Takayoshi Tagami[1], Hye-Jin Kang[1], Masayuki Okuyama[1], Nobuo Sakairi[3], Atsuo Kimura[1,*]

[1]Laboratory of Molecular Enzymology, Research Faculty of Agriculture, Hokkaido University, Sapporo 060-8589, Japan

[2]Department of Biotechnology, Faculty of Agro-Industry, Kasetsart University, Bangkok 10900, Thailand

[3]Division of Environmental Materials Science, Faculty of Environmental Earth Science, Hokkaido University, Sapporo 060-0810, Japan

[*]Corresponding author: tel/fax, +81 11 706 2808; e-mail addresses, kimura@abs.agr.hokudai.ac.jp (A. Kimura) and weranuch@abs.agr.hokudai.ac.jp (W. Lang).

E-mail addresses: weranuch@abs.agr.hokudai.ac.jp (W. Lang), sarote.s@ku.ac.th (S. Sirisansaneeyakul), tagami@abs.agr.hokudai.ac.jp (T. Tagami), hyejin@abs.agr.hokudai.ac.jp (H. J. Kang), okuyama@abs.agr.hokudai.ac.jp (M. Okuyama), nsaka@ees.hokudai.ac.jp (N. Sakairi), kimura@abs.agr.hokudai.ac.jp (A. Kimura).

Abstract

Lipophilic azo dyes are practically water-insoluble, and their dissolution by organic solvents and surfactants is harmful to biological treatment with living cells and enzymes. This study aimed to evaluate the feasibility of a newly synthesized nonreducing terminal chimeric isomaltomegalosaccharide (N-IMS) as a nontoxic solubilizer of four simulated lipophilic azo dye wastes for enzymatic degradation. N-IMS bearing a helical α-(1→4)-glucosidic segment derived from a donor substrate α-cyclodextrin was produced by a coupling reaction of cyclodextrin glucanotransferase. Inclusion complexing by N-IMS overcame the solubility issue with equilibrium constants of 1,786–242 M^{-1} (methyl yellow > ethyl red > methyl red > azo violet). Circular dichroism spectra revealed the axial alignment of the aromatic rings in the N-IMS cavity, while UV–visible absorption quenching revealed that the azo bond of methyl yellow was particularly induced. Desorption of the dyes from acidic and neutral soils was specific to aqueous organic over alkali extraction. The dissolution kinetics of the incorporated dyes followed a sigmoid pattern facilitating the subsequent decolorization process with azoreductase. It was demonstrated that after soil extraction, the solid dyes dissolved with N-IMS assistance and spontaneously digested by

coupled azoreductase/glucose dehydrogenase (for a cofactor regeneration system) with the liberation of the corresponding aromatic amine.

Keywords: azobenzene dye, biological treatment, chimeric structure, dye-contaminated soil remediation, saccharide solubilizer, methyl yellow

1. Introduction

Lipophilic azo dyes are persistent and accumulate in the environment, especially in sludge waste or soil near processing manufacturers, with a potential risk of carcinogenic effects and genotoxicity (Zanoni et al., 2013). Remediation of highly polluted sites with aromatic pollutants is complicated, as at least two essential series of soil washing and decomposition are mandatory (Fabbri, Prevot, Zelano, Ginepro, & Pramauro, 2008). To date, the removal of hydrophobic dyes by surfactants and organic solutions is common, followed by various recent technologies, such as electrochemical photocatalysis, ozonation, and Fenton oxidation (Muthuraman & Teng, 2009; Tehrani-Bagha & Holmberg, 2013; Hitam & Jalil, 2020). However, the latter drawbacks are the limitation of light penetration in colored effluents and the separation of fine catalysts from the treated medium (Fabbri et al., 2008). The biodegradation of water-soluble azo dyes under aerobic, anaerobic, and combined anaerobic-aerobic systems has been eagerly studied (O'Neill et al., 2000). Nevertheless, these approaches may face some limitations, e.g., larger land area and long operation time. In contrast, ex situ biological treatment with a microbial enzymatic system is a great advantage for highly specific dye degradation and elimination of deleterious byproducts regardless of land size (Husain, 2006). Although the critical step is to find an appropriate lipophilic dye solubilizer for exchanging organic solvents or surfactants after the soil extraction, this integration process has not been revealed before.

Azo dyes are synthetic colorants where the structure carries one or more chromophore azo groups (–N=N–) associated with benzene or naphthalene rings or sometimes with aromatic heterocycles, forcing them to have a core hydrophobic nature. Only anionic azo dye-substituted sulfonate (–O–SO_3Na) is highly water-soluble over the entire pH range, which has applicability in textile dyeing. The major class of anionic lipophilic azo dyes widely used as acid-base indicators, optical materials or chemosensors having carboxylate substituents, e.g., ethyl red (ER) and methyl red (MR), or hydroxyl groups, e.g., azo violet (AV), are only water-soluble in alkaline pH (Tehrani-Bagha & Holmberg, 2013). The opposite charge distribution in cationic azo dyes presented in amino substituents of the azobenzene dyes, e.g., methyl yellow (MY), is a consequence of alkali-insolubility (Matazo, Ando, Borin, Santos, 2008). As mentioned above, the solubilization of lipophilic dyes mostly requires surfactant, organic excipients, and pH adjustment with extreme acid or alkali (only for an ionizable dye) or an emulsion and a liposomal formulation,

most of which are highly susceptible to further enzymatic treatment, whereby lipophilic dye digestion can be more bioavailable if the dye states are maintained in a soluble form. Therefore, the remediation of lipophilic dyes by implementation with a mild solubilizer will be highly beneficial. In this context, pure nonvolatile saccharide solubilizers have been proposed, e.g., cyclic α-(1→4)-linked oligosaccharides (cyclodextrin; Song et al., 2019) and linear isomaltomegalosaccharide (L-IMS) with chimeric segments of short α-(1→4)-linkages at a reducing terminal of the α-(1→6)-glucosidic main chain (Lang et al., 2014a). Regarding the latter approach, we recently established the enzymatic synthesis approach of chimeric IMS bearing longer segments of α-(1→4) than L-IMS, and the physicochemical analysis emphasized the role of water solubility enhancement of poorly soluble compounds mainly arising from the α-(1→4)-segment (Lang et al., 2022a, b). Such knowledge influenced us to synthesize a new IMS structure by extending the length of the α-(1→4)-segment at the "nonreducing terminal" of the single IMS (N-IMS, Fig. 1A). N-IMS is hypothesized to incorporate a lipophilic molecule through host-guest interactions, and the complex is soluble in a water phase, similar to the properties of cyclodextrin. Furthermore, the helical chain of N-IMS is simplified to be digestible (with α-amylase) and expected to be safe for the biological purposes. N-IMS thus becomes the eco-friendly carbohydrate material having chimeric conformation with bifunctionality: the main chain of long α-(1→6)-segment contributes to the inherent high water solubility (Lang et al., 2022b), and the α-(1→4)-segment with helical chain supplies the specific inclusion ability. In addition, the oxygen-insensitive azoreductase (BrAzo) gene from *Brevibacillus laterosporus* TISTR1911 was cloned and overexpressed (Lang et al., 2013a). The enzyme appeared to have potential use as a long-term biocatalyst under the coupling of BrAzo and glucose dehydrogenase (GDH) for the regeneration of the cofactor β-nicotinamide adenine dinucleotide reduced form (NADH). This study aims to forward N-IMS as a lipophilic dye solubilizer and establish biotreatment of dye-contaminated soil using BrAzo/GDH for a potentially sustainable system.

In this study, we newly reported the synthesis of N-IMS in which the α-(1→4)-segment derived from α-cyclodextrin was introduced towards the α-(1→6)-main chain of a commercially available dextran T 10 by cyclodextrin glucanotransferase (CGTase; EC2.4.1.19) from *Bacillus macerans*. The putative helical conformation of the N-IMS and its hydrophobic binding capacity was evaluated by the formation of homogeneous complexes with iodine and fluorescence probe, 6-(*p*-toluidino)-2-naphthalene-6-sulfonate (TNS) in water, respectively. The intermolecular interaction was verified by the methods of continuous variation using Job's plots and two-dimensional (2D) ^{1}H-^{1}H nuclear overhauser enhancement spectroscopy (NOESY). The soil was adsorbed with AV, ER, MR, and MY (dye structures, see Fig. 2A) as representative site-polluted lipophilic dyes. We then investigated the basic principles of dye desorption from these soils with an alkaline and aqueous organic solvent combination. The specific binding capacity of the dye and N-

IMS complexes as well as the bioavailability test with the BrAzo coupling system for the decolorization of the incorporated dyes were discussed for the first time.

2 Materials and methods

2.1 Azo dyes, chemicals, and enzymes. Amylose (DP = 28, synthetic product; DP, average degree of polymerization) was purchased from Glico Nutrition (Osaka, Japan). Deuterium oxide (D_2O) was obtained from Kanto Chemical (Tokyo, Japan). TNS and deuterium chloride (35%, w/v, in D_2O) were purchased from Sigma–Aldrich (St. Louis, MO, USA). MR [4-(dimethylamino)azobenzene-2′-carboxylic acid], 4-dimethyl-*p*-phenylenediamine, and GDH (EC1.1.1.47) from *Bacillus* sp. were obtained from Wako Pure Chemical Industries (Osaka, Japan). ER [4-(diethylamino)azobenzene-2'-carboxylic acid], AV (synonym, magneson; 2,4-dihydroxyl-4'-nitroazobenzene), and MY [4-(dimethylamino)azobenzene] were obtained from Tokyo Chemical Industry (Tokyo, Japan). Dextran T 10 was purchased from Amersham Biosciences (Uppsala, Sweden) and fractionated to have DP of 48 (average value). α-Cyclodextrin and maltooctaose were a gift from Nihon Shokuhin Kako (Tokyo, Japan). CGTase (liquid form containing 13.8 ± 2.5 U/mL) was donated from Amano (Nagoya, Japan). For CGTase assay, enzyme diluted appropriately was incubated at 20 °C in 100 μL with 20 mM maltose and 20 mM α-cyclodextrin in 50 mM sodium acetate buffer, pH 5.5. The reaction mixture was withdrawn at 3, 10, and 20 min and heated at 100 °C for 10 min for termination of reaction. Maltooctaose of product was determined by high-performance anion-exchange chromatography with pulsed amperometric detection (HPAEC-PAD, Osaka Soda, Osaka, Japan) with a CarboPac PA1 column (Dionex, Sunnyvale, CA, USA) eluted with 640 mM NaOH solution supplemented with 10 mM sodium acetate. One unit of CGTase was defined as the amount of enzyme to produce 1 μmol maltooctaose by coupling α-cyclodextrin to maltose per min. *Myo*-inositol and maltooctaose were utilized as internal and external standards, respectively. Heterologous expression of dextran glucosidase from *Streptococcus mutans* by *Escherichia coli*, in which the enzyme catalyzes the exo-wise hydrolysis of dextran molecules at the terminus to release free glucose, was prepared in our laboratory (Saburi, Mori, Saito, Okuyama, & Kimura, 2006). α-Amylase (type I-A, EC3.2.1.1) from porcine pancrease, β-amylase (type II-B, EC3.2.1.2) from barley crude, and dextranse (EC3.2.1.11) from *Penicillium* sp. were obtained from Sigma–Aldrich. β-Nicotinamide adenine dinucleotide oxidized form (NAD^+) and other chemicals were purchased from Nacalai Tesque (Kyoto, Japan).

2.2 N-IMS synthesis. N-IMS was prepared according to the method in Patent no. 6655246 (Kimura, Hara, & Lang, 2020) with slight modification; dextran T 10 (9.6 g) and α-cyclodextrin (9.7 g) were dissolved by boiling in a microwave at the molar concentrations of 25 mM and 200 mM, respectively in 50 mL of 50 mM sodium acetate buffer, pH 6.0, and preincubation at 20 °C.

The reaction mixture was further incubated with CGTase (1 mL; 0.28 U/mL) for 3 h before boiling for 10 min. The mixture was subsequently incubated with dextran glucosidase (1 U/mL) at 37 °C for 24 h to digest the residual dextran T 10, boiled, and centrifuged at 11,300 ×*g* to obtain the supernatant. N-IMS in the supernatant was purified by precipitation with precooled methanol (60%, v/v), dialysis with a 3500 kDa Spectra/Por7 membrane (Rancho Dominguez, CA, USA) to remove glucose and oligosaccharides with DPs ≤21, and passage through a manually packed ion exchanger Amberlite MB-4 column (Organo, Tokyo, Japan) before freeze-drying.

2.3 Characterization of N-IMS. The linkage composition and DP were obtained by ^{1}H NMR and gel filtration HPLC analyses, respectively, according to previous methods (Lang et al., 2014a). The yield was determined by the amount of N-IMS divided by the amount of acceptor substrate (dextran T 10). Structure analysis of N-IMS using α-amylase treatment and gel filtration HPLC followed our previous methods of Lang et al. (2022a). Additionally, β-amylase and dextranase digests were performed similarly at pH 4.8 and 5.2, respectively. For an iodine staining assay, N-IMS (2 mg/mL in water, 125 μL) was mixed with iodine reagent (2.0 g iodine and 20.0 g potassium iodide in 1 L with water; freshly prepared; 5 μL), then fulfilled with 370 μL water, and allowed to stand for 5 min. The absorption spectra were monitored over the range of 350–800 nm without dilution (U2900 spectrophotometer, Hitachi, Tokyo, Japan). Synthetic amylose (DP = 28) was used as a reference. TNS is practically nonfluorescent in an aqueous solution but adapts a large fluorescence intensity in more hydrophobic environments (Beyer, Craig, & Gibbons, 1973). To determine the stability constant (K_c) of N-IMS, the complexes of 0.5 μM TNS with N-IMS (0, 1, 2, 4, 6, 8, and 10 mg/mL) in water were prepared by mixing them for 30 min in the dark at 25 °C and then transferred into 96-well black plate. The emission spectra were recorded from 400–550 nm by a fluorescence microplate reader (Tecan, Infinite M200-HAFH, Tokyo, Japan) at an excitation wavelength of 360 nm. The K_c value was calculated using Equation 1 according to the methods of Buranaboripan, Lang, Motomura, & Sakairi (2014) and Lang et al. (2022b):

$$\frac{1}{I-I_0} = \frac{1}{I'-I_0} + \frac{1}{K_c(I'-I_0)[H]} \qquad \text{(Equation 1)}$$

In the equation above, I_0, I, and I' are the initial fluorescence intensities of TNS without N-IMS, with N-IMS of different concentrations ([H]), and with N-IMS at the maximum concentration, respectively.

2.4 Solubility test of lipophilic dyes with N-IMS and inclusion analysis. Excess amounts of four dyes (AV, ER, MR, and MY; 1.0 mg) were mixed vigorously with 100 μL N-IMS at 0–10 mM (0, 2, 4, 6, 8, and 10 mM) in water at 25 °C for 4 h. The supernatant was collected by centrifugation at 12,000 ×*g* for 10 min three times. This portion was then diluted with 1 M NaOH solution, and the dye concentration was quantified by measuring the maximum absorptions (λ_{max}) at 556, 450, and

434 nm for AV, ER, and MR, respectively, using calibration curves constructed with the dye standards dissolved in 1 M NaOH. In the case of the MY test, DMSO was utilized instead with a λ_{max} of 425 nm. The equilibrium constant (K_s) was determined using Equation 2:

$$K_S = \frac{Slope}{S_0(1-Slope)} \qquad \text{(Equation 2)}$$

where the slope was obtained from the initial straight line of the plots of lipophilic dye concentrations against N-IMS concentrations (see Fig. 2B; open-circled plots), and S_0 is the solubility of the dye in water in the absence of N-IMS by following previous methods (Higuchi & Connors, 1965; Lang et al., 2014a). The same experiment was performed again with N-IMS at 0–50 mM (0, 10, 20, 30, 40, and 50 mM) in 50 mM Britton-Robinson buffer, pH 6.0, for comparison. Only for the MY test were the samples centrifuged before spectroscopic measurement to remove precipitant due to salts in buffer precipitated in DMSO. The influence of medium pH on the water solubility of MR was investigated in the pH range of 4.0–9.0 in 50 mM Britton-Robinson buffer with and without 10 mM N-IMS. Inclusion ability was estimated by recording the UV–vis spectra of N-IMS solution (0, 1, 5, 10, 15, and 20 mM) containing dyes as guest compounds (20, 40, and 35 μM for AV, ER, and MR, respectively, in 50 mM Britton-Robinson buffer, pH 6.0). The MY test was carried out at 40 μM in the same buffer at pH 2.0, as the dye is acid-soluble. For the conformational analysis, the dyes in excess were dissolved in 100 μL of 50 mM N-IMS dissolved in 50 mM Britton-Robinson buffer (pH 6.0). The soluble complexes (50 μL) were then taken and dried in vacuum. The dried complexes were dissolved in 0.5 mL water, and the circular dichroism spectra were recorded from 200–550 nm by a Jasco Ps-450 spectropolarimeter (Tokyo, Japan).

Stoichiometry of MY and N-IMS in the complexes was estimated based on a Job's plot method (Buranaboripan, Lang, Motomura, & Sakairi, 2014). The total concentration of N-IMS and MY was maintained constantly at 100 μM (i.e., [MY] + [N-IMS] = 100 μM) in 0.1 M Britton-Robinson buffer, pH 1.0. After standing for 15 min, the absorption spectra of a series of MY and N-IMS mixtures were recorded from 200–650 nm. The ΔAbs value at 318 or 512 nm (λ_{max}; see Fig. 4A) was obtained from the absorbance difference of MY in the presence and absence of N-IMS. In Job's plots, the x-axis value corresponds to the mol ratio of MY (*P*; see Fig. 4B), where *P* = [MY]/([MY] + [N-IMS]). The y-axis value becomes the ΔAbs multiplied by *P*. The MY complexed with the short-amylose (DP = 28) and α-cyclodextrin was prepared for comparison.

The ^{1}H NMR and 2D NOESY analyses were recorded for pure MY and its inclusion complex (formed from mixture of 20 mM MY and 20 mM N-IMS), respectively, at 298 K using a Bruker 500 MHz spectrometer. MY is soluble in acidic solution, however, the N-IMS-associated inclusion interaction might weaken the ionization of dye. Therefore, acidic condition was formed by dropwise-addition of deuterium chloride (5 μL) to dissolve about 2.25 mg of MY in 0.5 mL D_2O (20 mM MY) containing 20 mM N-IMS, and the solution pD measured afterward was 0.57. The

samples were kept overnight at 25 °C and centrifuged before analysis. For NOESY, the spectrum acquired a mixing time of 100 ms and 16 scans.

2.5 Preparation of artificial dye-contaminated soils (dye soil) and their desorption test. Moistureless garden soil was homogenized thoroughly in water, autoclaved at 121.5 °C for 15 min, washed with water three times, and dried in a vacuum (the so-called control soil). To mimic the soils contaminated with industrial discharge, two methods of soil treatment were prepared by applying initialized fixing dyes to the soils at 1.0 mg/g as follows. (1) Dyes adsorbed to acidic soil: the control soil (3 g) was suspended in 30 mL of 0.1 M sodium acetate buffer, pH 3.0, in three Falcon tubes and then mixed with AV, ER, and MR (3 mg, predissolved in 1 mL of 1 M NaOH. The tubes were mixed frequently by vortexing at 25 °C for 3 h. The dye soil was collected by centrifugation, repeatedly washed with water twice and dried. At this time, MY adsorption was skipped, as it is alkali-insoluble. (2) Dyes adsorbed to neutral soil: the above protocols were prepared identically, but all four dyes were dissolved in ethanol (1 mL) before placing them into the water-suspended control soils. To evaluate the efficiency of dye adsorption, the desorption of dye from (1) and (2) was performed by two methods. (i) Extraction by KOH. Dye soil and control soil (10 mg) were mixed with 1 mL of 0.1 M KOH in microtubes by vortexing for 4 h. The extracted portion was 400 μL after centrifugation at 3000 ×*g* for 10 min and acidified with 100 μL of 6 M hydrochloric acid. This allowed the dye to incorporate into the ethyl acetate layer (500 μL) after mixing by vortexing and centrifuging. The upper organic layer (100 μL) was taken and evaporated to dryness. The dye content in the dried portion was quantified following the methods described in Section 2.4. (ii) Extraction by chloroform + water + methanol + acetone immiscible solution (CWMA, 1:1:1:1, v/v) was carried out based on the best recovery data reported by Imran et al. (2015). Briefly, dye soil and control soil (10 mg) were mixed with CWMA by an ordered addition of 250 μL of chloroform, acetone, methanol, and water and mixed for 4 h. The lipophilic dyes were separated into the bottom layer of chloroform/acetone after centrifugation (3,000 ×*g*, 10 min). This portion was withdrawn (100 μL) and dried by speed-vacuum. The dye content determinations followed the methods described in Section 2.4, and DMSO was utilized for the MY test.

2.6 Azoreductase assays. Dye stocks (AV, ER, MR, and MY, 500 μM) were prepared in ethanol, and the solubility of dyes in enzymatic assays was maintained with 10% (v/v) ethanol in 50 mM Britton-Robinson buffer, pH 6.0. The BrAzo activity assay (1 mL) contained 100 μL dye stock (final dye concentration, 50 μM), 200 μM NADH, and BrAzo at 25 °C. One unit of BrAzo activity was defined as the amount of enzyme catalyzing the reduction of 1 μmol of dye per min (Lang et al., 2013a). BrAzo and GDH were coupled for the continuous generation of NADH. In this sharing

relationship, we measured the enzyme units of BrAzo and GDH by following the decrease and increase in the absorbance of NADH at 340 nm, respectively. The BrAzo activity assay contained 50 μM MR sodium salt, 200 μM NADH, and BrAzo, whereas the GDH assay contained 50 mM glucose, 200 μM NAD^+, and GDH. The activity units were defined as 1 μmol NADH oxidized or NAD^+ reduced per min, using an extinction coefficient of 6.3 $mM^{-1}cm^{-1}$ for BrAzo and GDH, respectively. In the Ping-Pong Bi-Bi mechanism, 2 mols of NADH are used to reduce 1 mol of azo dye via the NADH pathway (Bin et al., 2004); therefore, the unit concentrations of BrAzo and GDH were initially maintained at 1 and 2 U/mL throughout the study, respectively, as GDH was required to supply 2 mols of NADH to the BrAzo reaction for 1 mol of azo dye reduction.

2.7 Lipophilic dye decolorization in the coupling reaction of BrAzo/GDH/N-IMS

2.7.1 Decolorization of four dyes. The batch reaction mixture of N-IMS for dye dissolution and decolorization was determined with a 96-well plate through a Multiskan Ascent microplate reader (Thermo Fisher Scientific, Shanghai, China). The 100 μL assay was fixed with dried portions of 2 mM AV, ER, MR, and MY. To prepare this solid dye plate, 5 μL of 40 mM dye stock in ethanol solution was placed at one side of the well bottom, keeping the center clear for the possible well-read, and the plate was stored at 60 °C for 20 min to remove residual ethanol. Then, 100 μL of N-IMS solution at 0, 1, 5, 10, and 20 mM in 50 mM Britton-Robinson buffer, pH 6.0, was added to the well plate by a multichannel pipette. For the biodegradation test, the above N-IMS solutions were prepared identically but supplemented with glucose (50 mM) and transferred into the dried dye wells. Then, the enzymes (BrAzo 1 U/mL and GDH 2 U/mL) and NAD^+ (2 mM) were placed, and the plate was wrapped by a clear sheet. The shaking mode was started immediately at the beginning with 960 rpm for 10 s. The absorbance at 450 nm was autorecorded every 2 min for 120 min. The concentrations of dissolved dyes were calculated with the calibration curves. Sigmoid model parameters were obtained by fitting (Equation 3) with the experimental data of dissolved dye concentration (y) as a function of time (x) using Solver-based Microsoft Excel programming:

$$y = C_0 + \left(\frac{ax^b}{c^b + x^b}\right) \qquad \text{(Equation 3)}$$

where C_0 is the dye concentration. The a (μM) is C_M–C_0, where C_M (μM) represents the dye concentration at equilibrium. The b (μM/min) is the initial rate (slope) of solid dye transformation to a soluble form, and c (min) is the sigmoid midpoint or time point at which the sigmoidal curve reaches half of its maximum solubility. Consequently, the inclusion capacity of dyes in the N-IMS (q_N, mg/g) complex was calculated by Equation 4:

$$q_N = \left(\frac{aMW_{dye}V}{1000M_1}\right) \qquad \text{(Equation 4)}$$

where a is obtained from the Equation (3). M_1 is the mass of N-IMS utilized (mg) and V is the assay volume (1×10^{-4} L).

2.7.2 Decolorization process of MY extract. MY was scaled up for 1.6 g of neutral soil by CWMA solution (160 mL) following the protocol described in Section 2.5, filtrated to remove the residual soil by a GF/A glass microfiber filter (GE Healthcare, Buckinghamshire, UK), and dried. The dried portion was redissolved in methanol to adjust to an initial concentration of 2 mM, transferred to 1 mL into two microtubes and allowed to dry again by speed vacuum. Tube no. 1 was replenished with BrAzo/GDH and additives (1 mL) with the same composition and concentration of the assay in Section 2.7.1. Tube no. 2 was filled with BrAzo/GDH including additives and 20 mM N-IMS in 1 mL. The tubes were incubated at 25 °C with stirring by a ball-shaped magnetic bar. Portions of the reaction mixture (100 μL) were withdrawn (after 20 min and 1–3 days) and heated at 100 °C for 10 min to terminate the enzyme reaction. The aromatic amines were extracted with 100 μL of ethyl acetate, and the upper layer (50 μL) was taken after centrifugation at 12,000 ×g (10 min, 25 °C), dried, and redissolved in 50 μL of an HPLC mobile phase containing acetonitrile and 0.1% (v/v) phosphoric acid in the ratio of 3:7, v/v. The samples were subjected to HPLC analysis using the same instruments of Lang et al. (2014b) with a Cosmosil Cholester column (4.6 × 150 mm, Nacalai Tesque), and the isocratic eluent was run at 40 °C with a flow of 1 mL/min and a UV detector at 245 nm. 4-Dimethyl-*p*-phenylenediamine was used as an external standard.

3 Results and discussion

3.1 Synthesis and characterization of N-IMS. CGTase is known to catalyze an opening of cyclodextrin and subsequently transfer the linear dextrin towards the nonreducing end of the glucan acceptor (known as the coupling reaction) (Yoon & Robyt, 2006). In this study, CGTase was exploited to graft an α-(1→4)-segment of α-cyclodextrin donor molecules to dextran T 10 (DP = 48). The hydrophobicity was expected to arise from a stereochemical constraint of the new segment as the chain of sole α-(1→6)-glucosyl units of dextran is only highly hydrophilic. The increase of the peak area around the original dextran and decrease in about half of initial α-cyclodextrin in the reaction mixture were detectable in the gel filtration HPLC at the end of the CGTase reaction stage (Fig. 1B). The unreacted dextran would be next digested by dextran glucosidase into free glucose and completely removed by dialysis as well as the remained α-cyclodextrin. The ^{1}H NMR spectrum of purified N-IMS with the integration data is shown in Fig. S1. The obtained yield was 0.97 or 97%, w/w. N-IMS has an α-(1→4)-linkage composition of 29.0% in the chain of an average molecular weight of 8,100 Da, with a total DP of 50 comprising 15 and 35 units for α-(1→4)- and α-(1→6)-glucose, respectively. The structure of N-IMS was confirmed by treatment with the three enzymes of α-amylase, β-amylase, and dextranase. α-Amylase catalyzes the internal hydrolysis of

α-(1→4)-glycosidic segments containing three or more α-(1→4)-glucosyl moieties, resulting in the production of the mixture of maltose, maltotriose, and maltotetraose. β-Amylase is an exo-hydrolase to successively release maltose units from the nonreducing ends of α-(1→4)-linked chain. Dextranase is an endo-hydrolase that randomly hydrolyzes the α-(1→6)-linked substrate, resulting in the production of α-(1→6)-linked glucosaccharides. Resultant hydrolysates of N-IMS (Fig. S2A) digested with α-amylase and β-amylase were nearly identical. The peak area of N-IMS (retention time = 48.517 min; DP = 50) decreased by approximately 30%, and the retention time shifted to smaller values of 49.653 min (DP = 37; α-amylase) and 49.442 min (DP = 39; β-amylase). Results indicate that α-(1→4)-segment with at least DP = 13 (or 11) binds to the nonreducing end of α-(1→6)-segment, which almost agrees with DP = 15 expected previously for α-(1→4)-chain. Dextranase treatment displayed the loss of the original peak of N-IMS by the digestion of the α-(1→6)-main chain. The peak corresponded to DP = 15 of the α-(1→4)-segment was not clearly seen. It was likely eluted at leading-shoulder peak (about 53 min) of the main peak of isomaltooligosaccharides (59.575 min), or/and the maltodextrin with DP of 15 retrograded and was subsequently removed from sample solution. Fig. S2B shows the three enzymes-associated digestion models of N-IMS. Interestingly, CGTase preferentially reacts with smaller acceptor substrate of dextran (DP = 35) even for using dextran T 10 (average DP = 48). Actual size of dextran T 10 ranges from DP = 11 to DP = 250.

The proposed model structure of N-IMS was shown in Fig. 1A where the structural feature of N-IMS was subsequently discussed as follows. Iodine staining was used to qualify the inclusion property emerging from the new α-(1→4)-segment since it would be a negative color for the iodine complexed with both substrates of α-cyclodextrin and dextran but positive for amylose. Swanson (1948) suggested that the iodine color was related to the length of amylose in which iodine molecules were held lengthwise within the helix of six glucose residues per turn. The bathochromic shift from 490 to 568 nm (red to blue) was observed when dextrin/amylose chains are lengthened from 14.5 to over 45 glucose units (Bailey & Whelan, 1961). Consequently, the short-amylose with DP = 28 was used as a reference in this study since it maintains pure α-(1→4)-glycosidic linkage resulted in a purple color with a λ_{max} of 526 nm (Fig. 1C). Not surprisingly, the spectrum of N-IMS containing 15 units of α-(1→4)-glucosyl segment formed one-third of the maximum absorption of the short-amylose complex because the α-(1→4)-chain of N-IMS was shorter, and the λ_{max} was a slight shift to 530 nm. Furthermore, the fluorescence emission spectra of TNS were increased corresponding with the increasing concentrations of N-IMS and the K_c determined by the double-reciprocal plots (Fig. 1D and 1E) of N-IMS/TNS complexes was 125 M^{-1}, significantly higher than 14.8 M^{-1} of the L-IMS/TNS complex (Lang et al., 2022b). N-IMS thus possessed a sufficient hydrophobicity and we proposed its structural feature in merits with the lipophilic azo dye solubility in the next study.

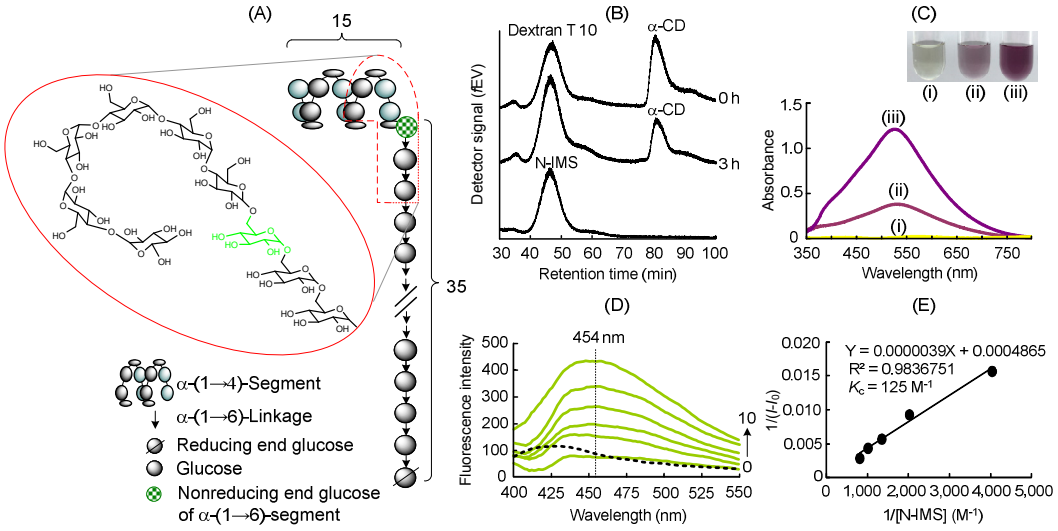

Fig. 1. (A) Model structure of nonreducing terminal isomaltomegalosaccharide (N-IMS). Green glucosyl residue represents the connecting part of dextran main chain to α-(1→4)-segment. (B) Gel filtration chromatograms of the enzymatic reactions at 0 and 3 h [incubated with α-cyclodextrin (α-CD) and dextran T 10 at 20 °C] and purified N-IMS. (C) UV-vis absorption scanned spectra of the iodine staining solution of α-cyclodextrin (i), N-IMS (ii), and short-amylose DP = 28 (iii) and their resulted color (inset). (D) Fluorescence spectra of TNS (0.5 μM) in the presence of N-IMS (0 mg/mL, dashed line; 1–10 mg/mL, green lines). Black arrow indicates the direction of the increasing concentrations of N-IMS. Dotted line depicts the emission wavelength at 454 nm. (E) The Benesi-Hildebrand double-reciprocal plots of the emission intensity at 454 nm against the series of N-IMS concentrations where the I_0 value was 87.5. K_c was calculated from the values of y-intercept/slope.

3.2 Solubility enhancement and inclusion ability. We evaluated the phase solubilities of four lipophilic dyes with increasing concentrations of N-IMS, and the results are shown in Table 1 and Fig. 2B. The K_s values determined with N-IMS concentrations of 0–10 mM in water were 1,786, 851, 491, and 242 M^{-1} for MY, ER, MR, and AV, respectively, depicting a stoichiometric ratio of 1:1 (N-IMS:dye), as it was the linear function corresponding to the A_L-type profile (Fig. 2B). N-IMS markedly improved the solubility of ER (with the K_s value of 851 M^{-1}) compared with the binding affinity with L-IMS in which the K_s value of 10 M^{-1} was previously determined (Lang et al., 2014a). According to buffers maintaining a constant pH for enzyme activity, we thus investigated the inclusion ability of N-IMS at higher concentrations in Britton-Robinson buffer at pH 6.0, as these constitute vital data for modeling enzymatic biotreatment. The results indicated that the solubilities of AV, ER and MR were slightly promoted by the buffer, as seen in the y-intercept

areas of Fig. 2B (a–c) and the values depicted in Table 1. Upon increasing the N-IMS concentration, the solubilities of AV, ER, and MR still increased proportionally with the A_L-type relationship, but the K_s values decreased to 89, 44, and 11 M^{-1} for AV, ER, and MR, respectively. In aqueous solution, free dyes can have different resonance structures and tautomer forms depending on the pH of the medium. Khouri, Abdel-Rahim, & Shamaileh (2013) reported the four forms of *m*-MR as *m*-MR^-, *m*-HMR, *m*-H_2MR^+, and *m*-$H_3MR^{+,}$ which are for the anionic (basic), mono-protonated (neutral), di-protonated (acidic), and tri-protonated (strongly acidic) forms, respectively. The basic forms are the most highly soluble for AV, ER, and MR but opposite to MY. MR is red in pH values under 4.4, yellow in pH values over 6.2, and orange in between: (red 4.2–6.2 yellow). The other dyes were also ionized and changed the colors: ER, red 4.9–7.0 yellow; AV, yellow 11.0–12.0 violet; and MY, red 2.9–4.0 yellow. In Fig. S3, the influence of medium pH (pH 6.0–9.0) on the phase solubility enhancement of MR indicates that the inherent solubility increases remarkably from 0.265 mM (pH 6.0) to 11.8 mM (pH 9.0) following our previous statement. However, the solubility enhancement by N-IMS was effective only at a pH range of 4.0–6.0, and the detraction was mainly seen at pH 9.0 (yielding a form of hydrazone). A similar relevant phenomenon was observed in Fig. 2B (a–c). It is suggested that AV, ER, and MR can adopt their hydrazone tautomeric forms under neutral conditions, resulting in slight solubility compared with their solubility in water, but this weakened the hydrophobic interaction inside the inclusion interior of N-IMS, resulting in decreases in the above K_s values. In contrast, MY solubility was never susceptible to neutral pH, but the phase solubility diagram likely followed the broad-bottom exponential A_P-type in the presence of increasing N-IMS concentrations (Fig. 2B (d)), yielding a higher K_s of 5,746 M^{-1} (Table 1). At high concentrations of N-IMS, in principle, more than one stoichiometry can be proposed for the binding of MY to the N-IMS cavity. Consequently, the basic intermolecular characterization by Job's plot and 2D NOESY was further discussed in the following section. The above result emphasized that the large free dyes that were always generated in the highly ionized state preferred to stay outside the N-IMS cavity. Despite this, MY could form a high-affinity complex and dissolve in neutral conditions only with N-IMS binding.

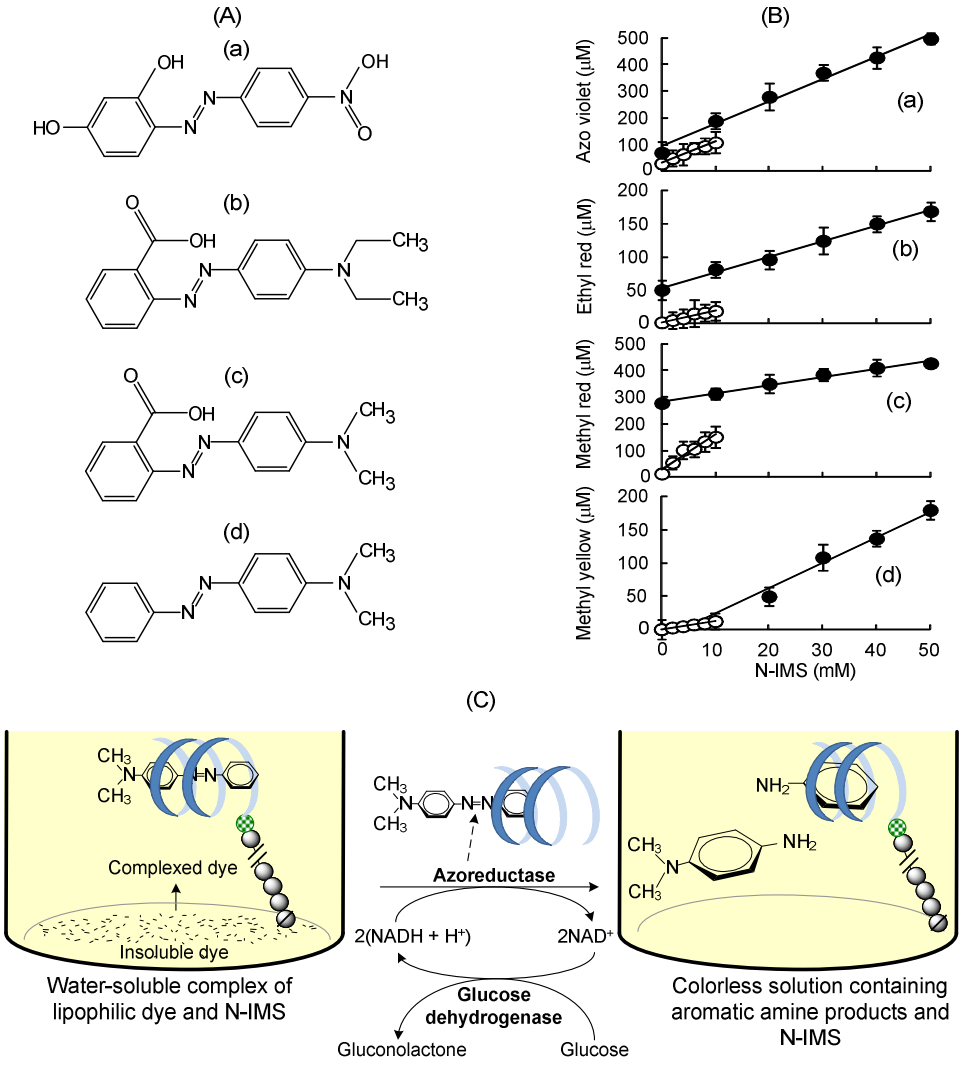

411

412 **Fig. 2.** (A) Chemical structures of the four lipophilic azo dyes used in this study: a, azo sviolet; b,
413 ethyl red; c, methyl red; d, methyl yellow. (B) Phase solubility diagrams of the dyes upon the
414 addition of N-IMS (0–10 mM) in water (○) and N-IMS (0–50 mM) in 50 mM Britton-Robinson
415 buffer, pH 6.0 (●). (C) Scheme of reactions taking place between methyl yellow and N-IMS and
416 digestion with an azoreductase coupling reaction.

417

418 **Table 1.** Equilibrium constants (K_s) of lipophilic dyes with N-IMS inclusion and the maximum
419 aqueous solubilities of lipophilic azo dyes in water and 50 mM Britton-Robinson buffer, pH 6.0.

Lipophilic dye	Water		Britton-Robinson buffer, pH 6.0	
	K_s (M^{-1})	Maximum solubility (μM)	K_s (M^{-1})	Maximum solubility (μM)
Azo violet	242	29.8 ± 3.6	89	95.2 ± 1.6
Ethyl red	851	2.1 ± 0.3	44	53.2 ± 3.2

Methyl red	491	14.0 ± 0.5	11	284.2 ± 7.3
Methyl yellow	1,786	0.7 ± 0.2	5,746	0.7 ± 0.2

The inclusion ability of N-IMS examined in terms of UV–vis spectroscopic titration (0–20 mM) using four lipophilic dyes as a guest compound is shown in Fig. 3 (A–D, top panels). The absorption maxima at visible wavelengths among AV, ER, and MR at pH 6.0 (with visible λ_{max} at 445, 450, and 430 nm, respectively) remained unchanged when increasing the N-IMS concentrations, but increasing intensities in UV regions were clearly observed for AV and MR, and those isosbestic points were formed at 363 and 345 nm, respectively. Khouri et al. (2013) revealed a decrease in the maximum absorption at 450 nm and a blueshift of approximately 20 nm in the UV–vis spectrum of *m*-MR with the addition of α-cyclodextrin in basic solution at pH 10.39, and the absorption in the UV region at 268 nm also decreased without any shift. Hence, their patterns are completely different from our MR incorporated in the N-IMS cavity.

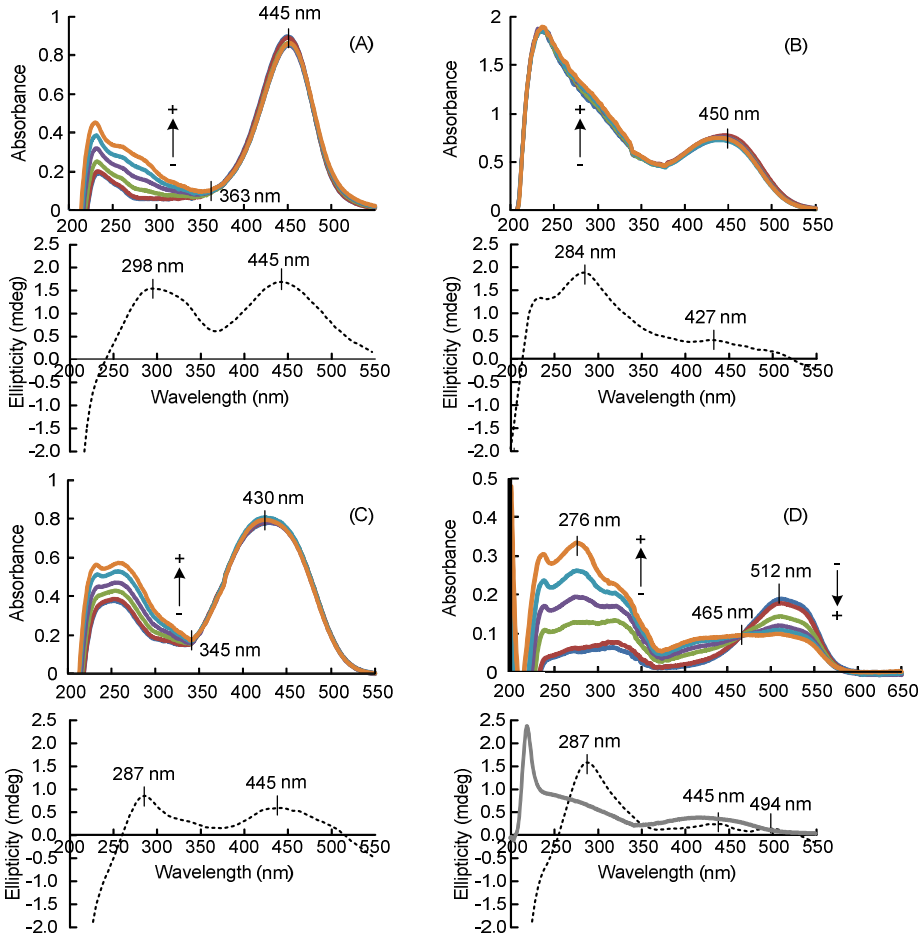

Fig. 3. Spectroscopic examination of the inclusion ability of N-IMS and the four lipophilic dyes: (A), azo violet; (B), ethyl red; (C), methyl red; (D), methyl yellow. Solvents: Britton-Robinson

buffer pH 6.0 (A–C) and pH 2.0 (D). (Upper panel) UV–vis spectra of the dyes in the presence of N-IMS (N-IMS concentration: 0, 1, 5, 10, 15, and 20 mM, read from - to +). (Lower panel) Circular dichroism spectra of the dyes (dashed lines) in the presence of N-IMS (50 mM in Britton-Robinson buffer, pH 6.0). Gray line in (D) is only the absorption spectrum of methyl yellow at pH 6.0.

Interestingly, the addition of N-IMS to an aqueous solution of MY at pH 2.0 resulted in a marked decrease in the intensity of the visible spectra of MY at 512 nm without any shift in its λ_{max} value (Fig. 3D, upper). In addition, the intensity in the UV region of 276 nm with a shoulder over 318 nm was significantly increased with the formation of an isobestic point at 465 nm. Ferreira and Ando (2012) assigned the bands of MY in acidic pH at 318 and 512 nm to azo and hydrazone tautomers, respectively, where hydrazone species are predominant. After inclusion with α-cyclodextrin, MY adapted the structure to be an azo tautomer, as the interior cavity precludes its protonation. It is clearly seen that the incorporation of MY with N-IMS inclusion has the same trend of spectrum quenching at 512 nm, suggesting that the inclusion of the azo bond penetrated deeply inside of the N-IMS cavity and kept the dimethylamino moiety outside as the proposed inclusion mechanisms of α-cyclodextrin. However, another absorption pattern of MY in the N-IMS cavity is completely different compared with the spectra of α-cyclodextrin. Similarly to amylose structure, the cavity of N-IMS may adopt a left-handed single helical conformation with its specific helix dimensions of 6–8 glucopyranose units per turn upon the complexation with ligands. Accordingly, it can be considered for approximately 2.5, 2.14, and 1.87 cyclic turns of the α-(1→4)-helical structure of DP = 15 segment for 6, 7, and 8 glucopyranose units, respectively, while the cavity of cyclodextrin is rigid with 1 turn. We explained the particularly different binding using the absorption spectra of MY derivatives measured at two pH values of 2.0 and 6.0, assigning 278 nm to aniline and a shoulder at approximately 312 nm to dimethyl-*p*-phenylenediamine bands (Fig. S4). Although the inclusion complexes of MY were performed at pH 2.0, the spectra observed in Fig. 3D were likely the combination of aniline and dimethyl-*p*-phenylenediamine spectra monitoring at pH 6.0, as seen in Fig. S4 (azo tautomer became predominant). The binding of N-IMS is more responsible for aniline because the 2.14 turns of the helix cavity may envelop the whole aniline molecule, resulting in an increase in the absorption intensity at 276 nm, where the aniline molecule may be almost released from the narrow rim of the α-cyclodextrin cavity when the azo bond deeply penetrates.

Next, the inclusion ability of N-IMS towards four dyes was revealed by the large positive induced circular dichroism effect observed at the main bands in the visible and UV regions. In the UV regions, the spectra were induced at 298, 284, 287, and 287 nm for AV, ER, MR, and MY, respectively, corresponding to the n–π* transition of the phenyl group. The Cotton effect (positive

chirality) ascribed to the π–π* transition of the azo linkage between the two benzene rings was presented at visible wavelengths of 445, 427, 445, and 445 nm for AV, ER, MR, and MY, respectively, corresponding to their visible absorption spectra with different degrees of ellipticity dependent on the induced fit of phenyl ring substituents. All of the data confirmed that the azobenzene dyes were incorporated into the N-IMS cavity with an axial orientation similar to the spectral pattern in the visible regions of the ER in the β-cyclodextrin cavity observed previously (Lang et al., 2014a). Variation in ratio of MY and N-IMS caused the energy transition of absorption maximum at 318 and 512 nm (Fig. 4A), coinciding with aniline and dimethyl-*p*-phenylenediamine bands, respectively. Stoichiometric ratio between MY and N-IMS showed the maximum variation of 0.5 at both λ_{max} (Fig. 4B), supporting the formation of 1:1-complex, which agreed with those of MY-amylose complex (0.5; Fig. 4C). Based on this manner, MY may penetrate deeply into the cylindrical cavity of N-IMS (2.14 helix turns) or short-amylose (DP = 28; 4 helix turns). But α-cyclodextrin exhibited the different maximum variation of 0.6 (Fig. 4C), implying the formation of 2:1-complex of MY and α-cyclodextrin. We have no clear explanation about this 2:1-complex conformation, but cavity of α-cyclodextrin might include the dimethylamino moiety of one MY and the phenyl ring of another MY.

As shown in Fig. 5A, the ^{1}H NMR assigns two types of MY protons: aliphatic protons $H_{\underline{a}}$ and aromatic protons $H_{\underline{b}}$–$H_{\underline{f}}$, and their chemical shifts of free or N-IMS-complexed state are shown in Table S1. By formation of MY-N-IMS complex, chemical shifts change in the following order: $H_{\underline{b}} > H_{\underline{f}} > H_{\underline{c}} > H_{\underline{d}} > H_{\underline{e}} > H_{\underline{a}}$ with $\Delta\delta$ values of 0.2233, 0.1530, 0.1518, 0.1406, 0.1020, and -0.0040 ppm, respectively, indicating that anomeric protons $H_{\underline{b}}$–$H_{\underline{f}}$ interact with N-IMS and $H_{\underline{a}}$ of dimethylamino group has no contact with N-IMS. The 2D NOESY estimated interaction sites of MY and N-IMS (Fig. 5B): the NOE correlations were observed between MY protons ($H_{\underline{b}}$, $H_{\underline{c}}$, $H_{\underline{e}}$, and $H_{\underline{f}}$) and N-IMS proton (H_5), whereas this evidence was not detected clearly in the aliphatic protons of dimethylamino group of $H_{\underline{a}}$ (Fig. S5) and the adjacent aromatic proton of $H_{\underline{d}}$ (Fig. 5B). Proton of H-5 is located inside of N-IMS similarly to β-CD (Nishizawa et al., 2014), and therefore this study demonstrates that an MY moiety exists inside of cavity of N-IMS to forms 1:1-complex. Conformational rearrangement of complex might accept deep penetration of azo bond and two phenyl rings. Two pheny moieties and azo bond of MY molecule are included with N-IMS, but dimethyl group is located outside of complex.

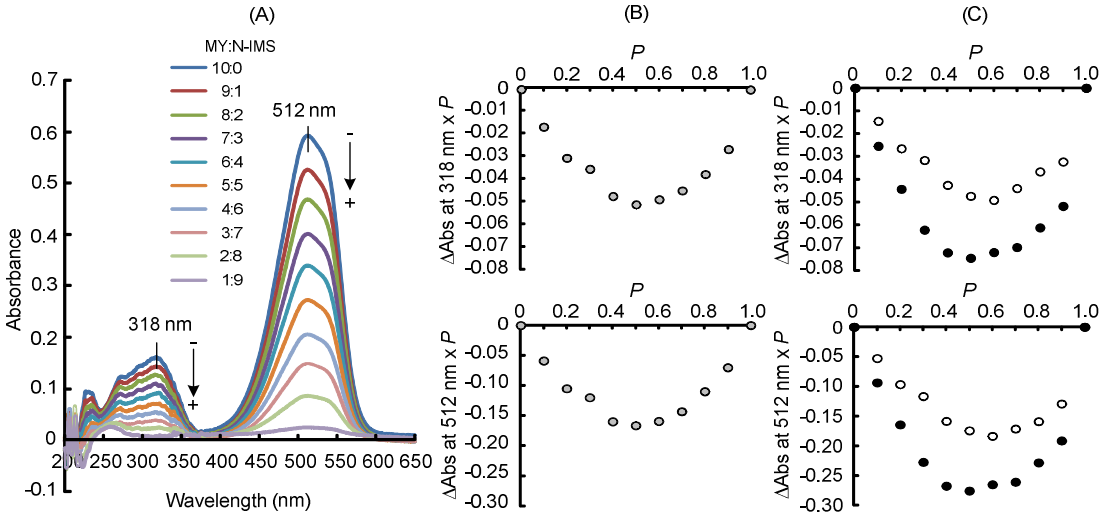

Fig. 4. (A) UV-vis spectra of methyl yellow (MY) in the presence of N-IMS. Concentration ratio of MY:N-IMS changed from 10:0 to 1:9, read from – to +. (B and C) Continuous variations of Job's method for the inclusion complex of methyl yellow and N-IMS (⊖), α-cyclodextrin (○), and short-amylose with DP = 28 (●) in 0.1 M Britton-Robinson buffer, pH 1.0. Upper and lower panels were obtained from ΔAbs at 318 and 512 nm, respectively, where the x-axis value corresponds to the mol ratio of MY: i.e., P = [MY]/([MY] + [N-IMS]).

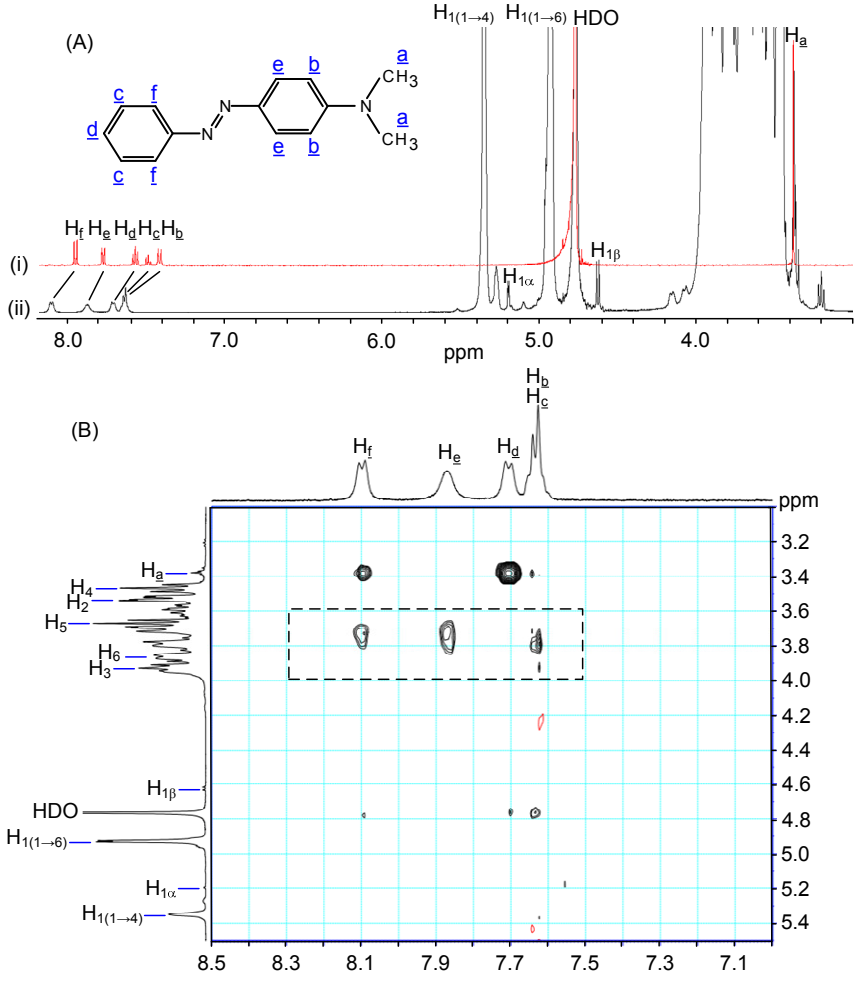

Fig. 5. (A) ^{1}H NMR spectra of MY (i) and its complex (ii) formed from 20 mM MY and 20 mM N-IMS under acidic conditions with 3.5 mg/mL deuterium chloride in D_2O. The a–f indicate the protons of MY. Solid lines between (i) and (ii) represent the protons, whose chemical shifts change by forming complex. (B) NOESY spectrum of the complex of MY and N-IMS (20 mM each) in the same solvent as show in Fig. 5A. Intermolecular NOEs are presented in the square.

3.3 Soil washing treatment. In this study, we considered the discharges of untreated effluents containing lipophilic dyes when dealing with their native medium. For example, alkali and organic agents are mainly supplied for anionic dyes, while organic media practically have general classes. However, unlike the binding of water-soluble dyes into soil, in which both substances can be incorporated in water systems (Imran et al., 2015), the incorporation of lipophilic dyes into soil in organic systems significantly minimizes their hydrophobic interaction. Moreover, the misbalance in the presence of incompatible solvent polarity and diluents may lead to reduced solubilization power and consequent precipitation. In our trials, we treated soils with acidic buffer (pH 3.0) and water (pH 6.8), which are always attractive electrostatic and hydrophobic interactions to the binding with

lipophilic dyes that were predissolved in 1 M NaOH and ethanol, respectively. As shown in Table 2, anionic dyes (AV, ER, and MR) potentially bound to the acidic soils (0.65–0.77 mg/g) with a slightly higher affinity than those same dyes (ethanol-based) amended to the neutral soils (0.42–0.70 mg/g). One of the possible reasons is that the functional groups of organic components of the soil surface (e.g., humic substance) can be protonated and deprotonated (e.g., –COOH, –OH, amine groups). At a consequent low pH, the binding of anionic species to soil charges becomes more positive (Nagy & Kónya, 2007). Not surprisingly, washing soil with the alkaline KOH effectively removed the dyes due to an increase in the electrostatic repulsion force, coincident with the previous desorption of anionic textile dyes by 0.1 M NaOH from the fungal beads (Lang et al., 2013b). However, the organic matter and oxides of silica and alumina also eluted spontaneously, as observed by the yellow–red color (Jozefaciuk, Muranyi, & Alekseeva, 2002). Moreover, the alkaline extraction of cationic lipophilic dye (i.e., MY) was unprofitable, as only 0.07 ± 0.01 mg MY/g was eluted, while the same sample extracted 0.89 ± 0.24 mg MY/g by CWMA solution without those interfering colors.

Table 2. Desorption of lipophilic azo dyes from acidic and neutral soils.

Desorbent	Dye	Acidic soil	Neutral soil
		Dye (mg/g)	Dye (mg/g)
Potassium hydroxide (0.1 M)	Azo violet	0.69 ± 0.04	0.70 ± 0.02
	Ethyl red	0.65 ± 0.11	0.62 ± 0.09
	Methyl red	0.77 ± 0.04	0.42 ± 0.00
	Methyl yellow	N.D.	0.07 ± 0.01
CWMA[a] (1:1:1:1, v/v)	Azo violet	0.84 ± 0.03	0.78 ± 0.09
	Ethyl red	0.73 ± 0.04	0.65 ± 0.05
	Methyl red	0.66 ± 0.04	0.61 ± 0.02
	Methyl yellow	N.D.	0.89 ± 0.24

N.D. = not determined because methyl yellow is insoluble in alkaline solution.

[a] Immiscible solution of chloroform + water + methanol + acetone.

Our attempt at alkaline extraction might be profitable in the sense of green treatment concepts to avoid organic disposal. In this concept, the alkaline extraction solution of those anionic dyes was able to be further neutralized to the optimum biological pH values by a strong acid, and after that, the enzymatic ingredients, including buffer and cofactor, could be formulated directly. However, the poor aqueous solubility of the extracted dyes was the major issue likely found in the case of high dye concentrations (typically ER, 2 mM), in which the precipitation was immediately visible at pH values lower than 7.68 (which could not eventually adjust to pH 6.0) because water

could not maintain solubilization. In addition, the fraction contaminated with unknown alkali-soluble substances may inhibit the enzyme activity. Furthermore, the adverse effects of soil after extreme acid and alkali treatments are permanent changes in coating minerals and organic matter content and result in a decrease in soil buffering capacity (Jozefaciuk et al., 2002). Taking into account these foregoing facts, we then selected CWMA as the aqueous organic model to wash the lipophilic dyes from soils because it was universal, and the solvents could be removed by evaporation (unlike surfactants), although the solvent efficiency with safety criteria is suggested to be more carefully considered. The following sections describe the dissolution kinetics by N-IMS assistance subsequent to the model treatment by enzymes (Fig. 2C).

3.4 Decolorization of dyes in N-IMS complexes. Wettability is the first step of any dissolution process to determine the interaction of solid and liquid surfaces, in which the latter is always water in the case of cyclodextrin-drug complexes, and both negative exponential and sigmoid type curves can be observed depending on the rate and degree of the wetting process (Szente & Szejtli, 1987). The dissolution patterns of the four dyes are presented in Fig. 6 (left column). N-IMS complexes carried the dyes from the solid-state at the bottoms of the well plates to the soluble form until the plateau of the dye saturation was reached at its maximum concentration (C_M). The solubility of solid dyes with N-IMS complexes was explained by Equation (3), as it gave rise to a sigmoid-shaped adsorption kinetic profile. In this equation, two parameters, *b* (rate) and *c* ($t_{1/2}$), can determine the rate-limiting step of the wettability, in which fast dissolution agrees with a large *b* and a small *c*. As seen in Table S2, among the four dyes, ER, with the largest *b*, 3.3–2.3 μM/min, and the smallest *c*, 7.4–35.3 min, was the rapidly soluble dye, whose *b* values decreased and *c* values gradually increased in the presence of N-IMS as the dyes needed the driving force to be incorporated. In addition, a higher N-IMS concentration provided more dissolved dye molecules, representing concentration capacity. All dyes showed increasing *a*, i.e., AV, 20.5–70.3 μM; ER, 40.2–73.1; MR, 207.6–310.0 μM; and MY, 0–67.8 μM, in accordance with increasing N-IMS concentration from 0–20 mM. Fig. 6C clearly supports the trends of *b* and *c* as mentioned. However, at the same time, *a* also increased with different levels. The degree of increase of *a* likely influenced Equation 3, resulting in a non-smooth tendency of some data in Table S2. The initial velocity of dye decolorization determined for BrAzo was in the order of ER > MR > AV > MY (196.5 ± 9.0 > 121.5 ± 0.5 > 26.3 ± 0.4 > 1.3 ± 0.0 U/mg). These degrees of enzyme activity reflected the invisible residual dye in the assay well plates because the addition of the BrAzo/GDH system could maintain the dye decolorization substantially, especially for AV, ER, and MR (Fig. 6B, 6D, and 6F). The incorporated dyes might react slowly with the enzyme, whereas the dissolving dyes might react more smoothly. Even in slow reaction, the process could be eventually completed with the appropriate incubation time and stirring control. Decolorization of MY (Fig. 6H)

in the presence of N-IMS was the slowest because BrAzo showed less specificity (151-fold lower than the ER activity). Moreover, the azo bond of MY penetrated deeply into the N-IMS cavity (as discussed in Section 3.2), consequently accessible to BrAzo only after the dye azo bond was released to the outside of complex (see equilibrium between two states shown in the left and center panels in Fig. 2C). This is a dynamic process whereby the guest molecule continuously associates and dissociates from the host molecules.

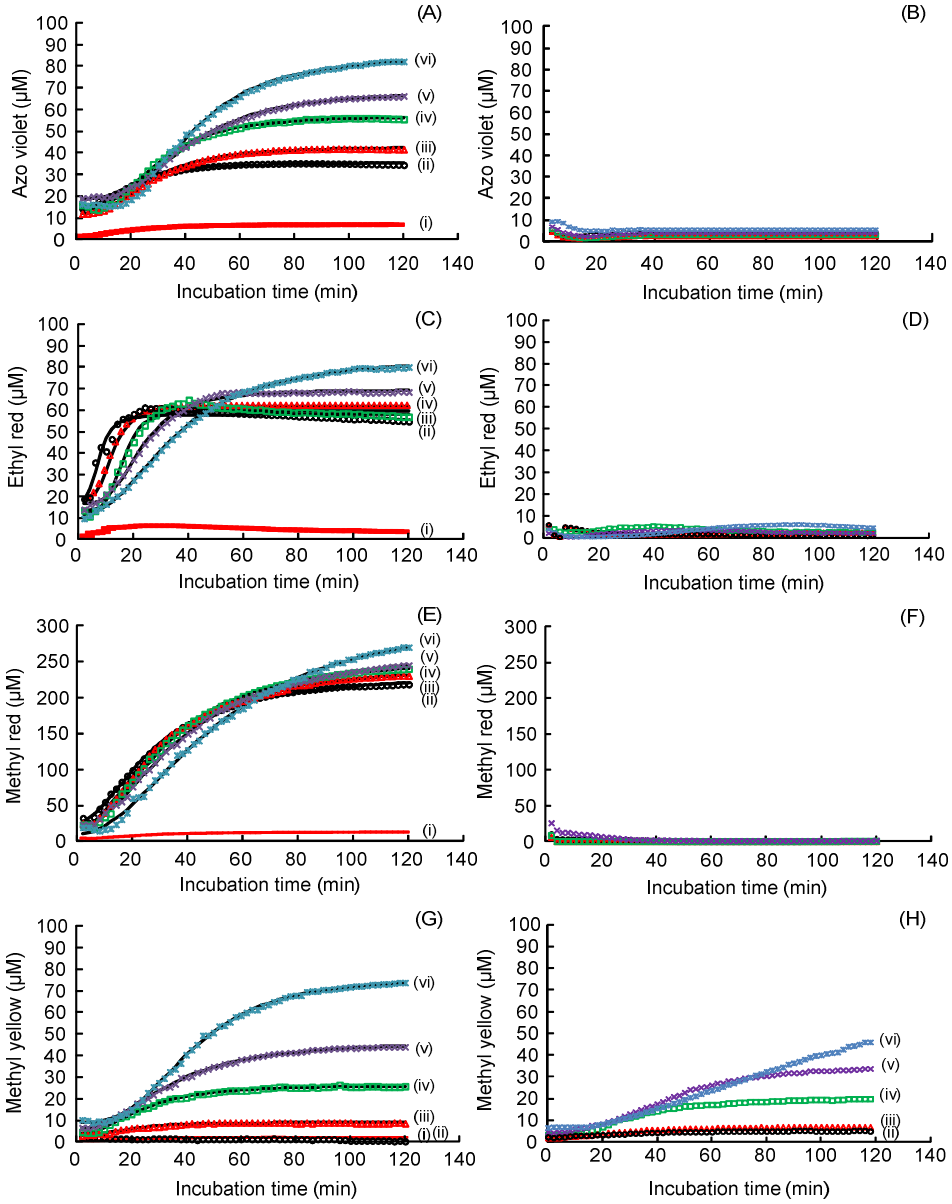

Fig. 6. (Left column) Sigmoidal dissolution kinetics of the four solid lipophilic dyes, (A), azo violet; (C), ethyl red; (E), methyl red; and (G), methyl yellow in water (i) and in the presence of N-IMS from 0 (ii); 1 (iii); 5 (iv); 10 (v); and 20 (vi) mM dissolved in 50 mM Britton-Robinson buffer,

pH 6.0. Lines of (ii)–(iv) represent the nonlinear curve fit from Equation (3). (Right column) Coupling enzymatic decolorization kinetics of the four solid lipophilic dyes, (B), azo violet; (D), ethyl red; (F), methyl red; and (H), methyl yellow in the presence of N-IMS from 0–20 mM (ii–vi) in 50 mM Britton-Robinson buffer, pH 6.0.

After incubating the enzymes and 20 mM N-IMS in the tube containing dried extracted MY with stirring, it was observed that the clear, bright yellow color arose from the tube bottom, while the yellow color in the tube without N-IMS was less visible as certain dye still bound to the tube. MY has two aromatic amine metabolites, aniline (colorless) and dimethyl-*p*-phenylenediamine (brown). After 1 day, the shade of the sample color changed to brown, implying that MY was consumed from both tubes, with a slightly higher color in the N-IMS medium (Fig. 7). After 2 days, the concentrations of dimethyl-*p*-phenylenediamine became almost equal and stabilized, indicating that N-IMS improved the bioavailability of MY digestion in the initial stage. The reason for the unchanged amount of aromatic amine might come from the glucose depletion in the reaction as all glucose molecules might be oxidized to gluconolactone by GDH in a coupled reaction to generate NADH (Fig. 2C). Long-term intermittent glucose feeding is suggested but we cannot explain why dimethyl-*p*-phenylenediamine decreased after some time. Considering the inclusion ability of N-IMS in the presence of high aromatic dye concentrations, the aromatic moieties of the substrate and products could be competitively occupied by the N-IMS cavity corresponding to the degree of hydrophobic attraction, eventually preventing the solubility enhancement activity of N-IMS. We suggest the coupling of one more enzyme that can mineralize aromatic amine products or alter the metabolite shapes to be inappropriate with the N-IMS cavity (e.g., macromolecule products catalyzed by laccase or peroxidase), as the sequential inclusion of the dye substrate can be smoother.

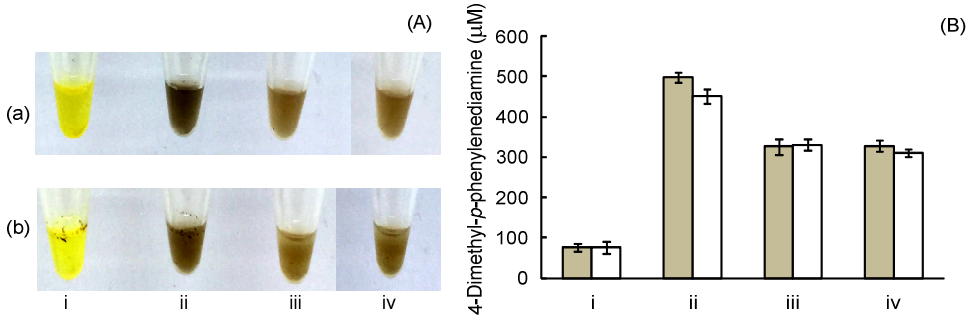

Fig. 7. Analysis of the digestion products of methyl yellow extract by the integration of N-IMS and azoreductase from *Brevibacillus laterosporus* TISTR1911 coupled with glucose dehydrogenase (a) at 20 min (i), 24 h (ii), 48 h (iii), and 72 h (iv). The process without N-IMS addition is presented

for comparison (b). (A) Color changes in the sampling tubes. (B) Detection of 4-dimethyl-*p*-phenylenediamine with N-IMS (gray bars; a) and without N-IMS (white bars; b).

4. Conclusion

In this study, we synthesized N-IMS with a DP of 50 and 29.0% α-(1→4)-linkages by the coupling reaction of CGTase. N-IMS bearing the α-(1→4)-helical segment at its nonreducing end to form cavity was responsible for the specific inclusion ability and improved the aqueous solubility of lipophilic azo dyes. The cavity of N-IMS could incorporate the water-insoluble azo dye ligand and formed the guest-host complex in 1:1 ratio with MY and N-IMS, where MY was located on the inside of cavity. Furthermore, N-IMS contributed to preventing the precipitation formation of dye extracted from soil-contaminated samples. The eco-friendly decolorization system of the dyes was established with N-IMS as pure and safe saccharide solubilizer under the coupling of BrAzo and GDH. Chimeric N-IMS is also profitable for drug delivery approaches and designing foods.

Acknowledgments

We thank Assistant Professor Rakrudee Sarthima, Mahasarakham University, Thailand, for the preliminary study of azoreductase, azo dyes, and megalosaccharides. This study was partially supported by a Program for Promotion of Basic and Applied Research for Innovations in Bioriented Industry (BRAIN), Japan [Grant numbers 25001A, 26062B] and the Japan Society for the Promotion of Science KAKENHI [Grant numbers 17H03801, 19KK0147]. The manuscript received an English proof from Elsevier's Author Services.

CRediT authorship contribution statement

Weeranuch Lang: Conceptualization, Investigation, Formal analysis, Writing - original draft, review & editing. Sarote Sirisansaneeyakul: Supervision, Validation. Takayoshi Tagami: Resources, Supervision. Hye-Jin Kang: Formal analysis, Investigation. Masayuki Okuyama: Data curation, Resources. Nobuo Sakairi: Conceptualization, Supervision. Atsuo Kimura: Writing - review & editing, Resources, Supervision, Funding acquisition, Project administration.

Declaration of competing interest. The authors have no conflicts of interest to declare.

References

Bailey, J. M., & Whelan, W. J. (1961). Physical properties of starch. I. Relationship between iodine stain and chain length. *Journal of Biological Chemistry*, *236*(4), 969–973. https://doi.org/10.1016/S0021-9258(18)64226-7

664 Bin, Y., Jiti, Z., Jing, W., Cuihong, D., Hongman, H., Zhiyong, S., & Yongming, B. (2004).
665 Expression and characteristics of the gene encoding azoreductase from *Rhodobacter*
666 *sphaeroides* AS1.1737. *FEMS Microbiology Letters*, *236*(1), 129–136.
667 https://doi.org/10.1016/j.femsle.2004.05.034
668 Buranaboripan, W., Lang, W., Motomura, E., & Sakairi, N. (2014). Preparation and
669 characterization of polymeric host molecules, β-cyclodextrin linked chitosan derivatives
670 having different linkers. *International Journal of Biological Macromolecules*, *69*, 27–34.
671 https://doi.org/10.1016/j.ijbiomac.2014.05.016
672 Fabbri, D., Prevot, A. B., Zelano, V., Ginepro, M., & Pramauro, E. (2008). Removal and
673 degradation of aromatic compounds from a highly polluted site by coupling soil washing with
674 photocatalysis. *Chemosphere*, *71*(1), 59–65.
675 https://doi.org/10.1016/j.chemosphere.2007.10.028
676 Ferreira, I. R., & Ando, R. A. (2012). Shifting the Azo-hydrazone tautomeric equilibrium of methyl
677 yellow in acidic medium by the formation of inclusion complexes with cyclodextrins.
678 *Chemical Physics Letters*, *522*, 51–53. https://doi.org/10.1016/j.cplett.2011.12.011
679 Higuchi, T., & Connors, A. (1965). Phase-solubility techniques. *In: Reilly CN, Editor. Advances in*
680 *Analytical Chemistry Instrumentation. Vol. 4. New York, NY: Interscience*, *4*, 117–212.
681 Hitam, C. N. C., & Jalil, A. A. (2020). A review on exploration of Fe_2O_3 photocatalyst towards
682 degradation of dyes and organic contaminants. *Journal of Environmental Management*, *258*,
683 110050. https://doi.org/10.1016/j.jenvman.2019.110050
684 Husain, Q. (2006). Potential applications of the oxidoreductive enzymes in the decolorization and
685 detoxification of textile and other synthetic dyes from polluted water: A review. *Critical*
686 *Reviews in Biotechnology*, *26*(4), 201–221. https://doi.org/10.1080/07388550600969936
687 Imran, M., Shaharoona, B., Crowley, D. E., Khalid, A., Hussain, S., & Arshad, M. (2015). The
688 stability of textile azo dyes in soil and their impact on microbial phospholipid fatty acid
689 profiles. *Ecotoxicology and Environmental Safety*, *120*, 163–168.
690 https://doi.org/10.1016/j.ecoenv.2015.06.004
691 Jozefaciuk, G., Muranyi, A., & Alekseeva, T. (2002). Effect of extreme acid and alkali treatment
692 on soil variable charge. *Geoderma*, *109*(3–4), 225–243. https://doi.org/10.1016/S0016-
693 7061(02)00177-5
694 Kimura, A., Hara, H., & Lang, W. (2020). Production methods and application of
695 isomaltomegalosaccharides having double- or single-anchor and use thereof. Japan Patent no.
696 6655246.
697 Khouri, S. J., Abdel-Rahim, I. A., & Shamaileh, E. M. (2013). A thermodynamic study of α-, β-,
698 and γ-cyclodextrin-complexed *m*-methyl red in alkaline solutions. *Journal of Inclusion*
699 *Phenomena and Macrocyclic Chemistry*, *77*(1–4), 105–112. https://doi.org/10.1007/s10847-

012-0221-x

Lang, W., Sirisansaneeyakul, S., Ngiwsara, L., Mendes, S., Martins, L. O., Okuyama, M., & Kimura, A. (2013a). Characterization of a new oxygen-insensitive azoreductase from *Brevibacillus laterosporus* TISTR1911: Toward dye decolorization using a packed-bed metal affinity reactor. *Bioresource Technology*, *150*, 298–306. https://doi.org/10.1016/j.biortech.2013.09.124

Lang, W., Buakaew, P., Buranaporipan, W., Wongchawalit, J., Sakairi, N., Vanichsriratana, W., & Sirisansaneeyakul, S. (2013b). Biosorption of local textile dyes onto acid-tolerant macro-beads of chitosan-immobilized Rhizopus arrhizus biomass. *Kasetsart Journal - Natural Science*, *114*, 101–114.

Lang, W., Kumagai, Y., Sadahiro, J., Maneesan, J., Okuyama, M., Mori, H., Sakairi, N., & Kimura, A. (2014a). Different molecular complexity of linear-isomaltomegalosaccharides and β-cyclodextrin on enhancing solubility of azo dye ethyl red: Towards dye biodegradation. *Bioresource Technology*, *169*, 518–524. https://doi.org/10.1016/j.biortech.2014.07.025

Lang, W., Sirisansaneeyakul, S., Martins, L. O., Ngiwsara, L., Sakairi, N., Pathom-aree, W., Okuyama, M., Mori, H., & Kimura, A. (2014b). Biodecolorization of a food azo dye by the deep sea *Dermacoccus abyssi* MT1.1^{T} strain from the Mariana Trench. *Journal of Environmental Management*, *132*, 155–164. https://doi.org/10.1016/j.jenvman.2013.11.002

Lang, W., Kumagai, Y., Sadahiro, J., Saburi, W., Sarnthima, R., Tagami, T., Okuyama, M., Mori, H., Sakairi, N., Kim, D., & Kimura, A. (2022a). A practical approach to producing isomaltomegalosaccharide using dextran dextrinase from *Gluconobater oxydans* ATCC 11894. *Applied Microbiology and Biotechnology*, *106*, 689–698. https://doi.org/10.1007/s00253-021-11753-6

Lang, W., Kumagai, Y., Habu, S., Sadahiro, J., Tagami, T., Okuyama, M., Kitamura, S., Sakairi, N., & Kimura, A. (2022b). Physicochemical functionality of chimeric isomaltomegalosaccharides with α-(1 → 4)-glucosidic segments of various lengths. *Carbohydrate Polymers*, *291*, 119562. https://doi.org/10.1016/j.carbpol.2022.119562

Matazo, D. R. C., Ando, R. A., Borin, A. C., & Santos, P. S. (2008). Azo-hydrazone tautomerism in protonated aminoazobenzenes: Resonance Raman spectroscopy and quantum-chemical calculations. *Journal of Physical Chemistry A*, *112*(19), 4437–4443. https://doi.org/10.1021/jp800217c

Muthuraman, G., & Teng, T. T. (2009). Extraction of methyl red from industrial wastewater using xylene as an extractant. *Progress in Natural Science*, *19*(10), 1215–1220. https://doi.org/10.1016/j.pnsc.2009.04.002

Nagy, N. M., & Kónya, J. (2007). Study of pH-dependent charges of soils by surface acid-base properties. *Journal of Colloid and Interface Science*, *305*(1), 94–100.

https://doi.org/10.1016/j.jcis.2006.09.040
Nishizawa, M., Hosoya, T., Hirokawa, T., Shin-Ya, K., & Kumazawa, S. (2014). NMR spectroscopic characteriation of inclusion complexes of theaflavin digallate and cyclodextrins. *Food Science and Technology Research, 20*(3), 663-669. https://doi.org/10.3136/fstr.20.663
O'Neill, C., Lopez, A., Esteves, S., Hawkes, F. R., Hawkes, D. L., & Wilcox, S. (2000). Azo-dye degradation in an anaerobic-aerobic treatment system operating on simulated textile effluent. *Applied Microbiology and Biotechnology*, *53*(2), 249–254. https://doi.org/10.1007/s002530050016
Saburi, W., Mori, H., Saito, S., Okuyama, M., & Kimura, A. (2006). Structural elements in dextran glucosidase responsible for high specificity to long chain substrate. *Biochimica et Biophysica Acta*, *1764*, 688–698. https://doi.org/10.1016/j.bbapap.2006.01.012
Song, P., Feng, W., Shi, H., Zhao, J., Liu, R., & Xu, W. (2019). Efficient decolorization of water and oil-soluble Azo dyes by enterococcus avium treated with HP-β-CD. *Pakistan Journal of Zoology*, *51*(2), 675–680. https://doi.org/10.17582/journal.pjz/2019.51.2.675.680
Swanson, M. A. (1948). Studies on the structure of polysaccharides. IV. Relation of the iodine color to the structure. *Journal of Biological Chemistry*, *172*(2), 825–837. https://doi.org/10.1016/s0021-9258(19)52772-7
Szente, L., & Szejtli, J. (1987). Wettability of cyclodextrin complexes. *Acta Pharmaceutica Hungarica*, *57*(1), 73–76.
Tehrani-Bagha, A. R., & Holmberg, K. (2013). Solubilization of hydrophobic dyes in surfactant solutions. *Materials*, *6*(2), 580–608. https://doi.org/10.3390/ma6020580
Yoon, S. H., & Robyt, J. F. (2006). Optimized synthesis of specific sizes of maltodextrin glycosides by the coupling reactions of *Bacillus macerans* cyclomaltodextrin glucanyltransferase. *Carbohydrate Research*, *341*(2), 210–217. https://doi.org/10.1016/j.carres.2005.11.014
Zanoni, T. B., Lizier, T. M., Assis, M. das D., Zanoni, M. V. B., & De Oliveira, D. P. (2013). CYP-450 isoenzymes catalyze the generation of hazardous aromatic amines after reaction with the azo dye Sudan III. *Food and Chemical Toxicology*, *57*, 217–226. https://doi.org/10.1016/j.fct.2013.03.035

Figure captions

Fig. 1. (A) Model structure of nonreducing terminal isomaltomegalosaccharide (N-IMS). Green glucosyl residue represents the connecting part of dextran main chain to α-(1→4)-segment. (B) Gel filtration chromatograms of the enzymatic reactions at 0 and 3 h [incubated with α-cyclodextrin (α-CD) and dextran T 10 at 20 °C] and purified N-IMS. (C) UV-vis absorption scanned spectra of the iodine staining solution of α-cyclodextrin (i), N-IMS (ii), and short-amylose DP = 28 (iii) and their

resulted color (inset). (D) Fluorescence spectra of TNS (0.5 μM) in the presence of N-IMS (0 mg/mL, dashed line; 1–10 mg/mL, green lines). Black arrow indicates the direction of the increasing concentrations of N-IMS. Dotted line depicts the emission wavelength at 454 nm. (E) The Benesi-Hildebrand double-reciprocal plots of the emission intensity at 454 nm against the series of N-IMS concentrations where the I_0 value was 87.5. K_c was calculated from the values of y-intercept/slope.

Fig. 2. (A) Chemical structures of the four lipophilic azo dyes used in this study: a, azo violet; b, ethyl red; c, methyl red; d, methyl yellow. (B) Phase solubility diagrams of the dyes upon the addition of N-IMS (0–10 mM) in water (○) and N-IMS (0–50 mM) in 50 mM Britton-Robinson buffer, pH 6.0 (●). (C) Scheme of reactions taking place between methyl yellow and N-IMS and digestion with an azoreductase coupling reaction.

Fig. 3. Spectroscopic examination of the inclusion ability of N-IMS and the four lipophilic dyes: (A), azo violet; (B), ethyl red; (C), methyl red; (D), methyl yellow. Solvents: Britton-Robinson buffer pH 6.0 (A–C) and pH 2.0 (D). (Upper panel) UV–vis spectra of the dyes in the presence of N-IMS (N-IMS concentration: 0, 1, 5, 10, 15, and 20 mM, read from - to +). (Lower panel) Circular dichroism spectra of the dyes (dashed lines) in the presence of N-IMS (50 mM in Britton-Robinson buffer, pH 6.0). Gray line in (D) is only the absorption spectrum of methyl yellow at pH 6.0.

Fig. 4. (A) UV-vis spectra of methyl yellow (MY) in the presence of N-IMS. Concentration ratio of MY:N-IMS changed from 10:0 to 1:9, read from – to +. (B and C) Continuous variations of Job's method for the inclusion complex of methyl yellow and N-IMS (⊙), α-cyclodextrin (○), and short-amylose with DP = 28 (●) in 0.1 M Britton-Robinson buffer, pH 1.0. Upper and lower panels were obtained from ΔAbs at 318 and 512 nm, respectively, where the x-axis value corresponds to the mol ratio of MY: i.e., P = [MY]/([MY] + [N-IMS]).

Fig. 5. (A) ^{1}H NMR spectra of MY (i) and its complex (ii) formed from 20 mM MY and 20 mM N-IMS under acidic conditions with 3.5 mg/mL deuterium chloride in D_2O. The a–f indicate the protons of MY. Solid lines between (i) and (ii) represent the protons, whose chemical shifts change by forming complex. (B) NOESY spectrum of the complex of MY and N-IMS (20 mM each) in the same solvent as show in Fig. 5A. Intermolecular NOEs are presented in the square.

Fig. 6. (Left column) Sigmoidal dissolution kinetics of the four solid lipophilic dyes, (A), azo violet; (C), ethyl red; (E), methyl red; and (G), methyl yellow in water (i) and in the presence of N-

IMS from 0 (ii); 1 (iii); 5 (iv); 10 (v); and 20 (vi) mM dissolved in 50 mM Britton-Robinson buffer, pH 6.0. Lines of (ii)–(iv) represent the nonlinear curve fit from Equation (3). (Right column) Coupling enzymatic decolorization kinetics of the four solid lipophilic dyes, (B), azo violet; (D), ethyl red; (F), methyl red; and (H), methyl yellow in the presence of N-IMS from 0–20 mM (ii–vi) in 50 mM Britton-Robinson buffer, pH 6.0.

Fig. 7. Analysis of the digestion products of methyl yellow extract by the integration of N-IMS and azoreductase from *Brevibacillus laterosporus* TISTR1911 coupled with glucose dehydrogenase (a) at 20 min (i), 24 h (ii), 48 h (iii), and 72 h (iv). The process without N-IMS addition is presented for comparison (b). (A) Color changes in the sampling tubes. (B) Detection of 4-dimethyl-*p*-phenylenediamine with N-IMS (gray bars; a) and without N-IMS (white bars; b).